Science Arts & Métiers (SAM)
is an open access repository that collects the work of Arts et Métiers Institute of Technology researchers and makes it freely available over the web where possible.

This is an author-deposited version published in: https://sam.ensam.eu
Handle ID: .http://hdl.handle.net/10985/21835

To cite this version :

Guillaume FASSE, Gregory GERMAIN, Florent BECKER, Frederic HAUVILLE - Development of an Experimental Blade-controlled Cycloidal Propeller - In: Congrès Français de Mécanique, France, 2019-08 - Congrès Français de Mécanique - 2019

Any correspondence concerning this service should be sent to the repository Administrator : scienceouverte@ensam.eu

Development of an Experimental Blade-controlled Cycloidal Propeller

G. FASSE[a*], F. HAUVILLE[a], G. GERMAIN[b], J-A. ASTOLFI[a], F. BECKER[a]

a. Naval Academy Research Institute (IRENav), BCRM Brest, CC600, 29240 Brest Cedex9, France
b. Ifremer, Marine Structure Laboratory 62200 Boulogne-sur-Mer, France
* guillaume.fasse@ecole-navale.fr

Abstract

As an interesting naval propulsion systems, this paper presents the development of an experimental cycloidal propeller. Cross-flow propellers are characterized by the rotation of several blades around a vertical axis associated with a movement of each blade around its axis (blade pitching). Two kinematic modes depending on the advance coefficient λ are distinguished: cycloidal mode for low ship speeds ($\lambda < 1$) and trochoidal mode for high speeds ($\lambda > 1$). The final goal is to establish pitch laws, for each of those two modes, dealing with a target optimization (thrust maximizing for example)[1]. For this purpose, an experimental thruster designed at the IRENav[2, 3, 4] can perform more or less complicated pitch laws thanks to three servo motor controlling each blade independently. Kinematics of cycloid propellers is first outlined and pitch laws are defined by a quasi-static approach. Then Ifremer facilities of Boulogne-sur-Mer are presented. Experimental thruster is described as its current blade-control system. Finally improvements on the electronic command are proceeded through the development of a Digital Twins and a test bench.

Key words : Naval propulsion, vertical axis, blade control

1 Introduction

For the last two decades, innovative naval propulsion systems have been investigated thanks to the growing development of unmanned underwater vehicles. Cross-flow propellers are promising alternative concepts from usual screw propellers. These devices take energy from unsteady hydrodynamic forces generated by blades oscillation or heaving like natural marine animal swimmers (biomimetism)[5].
Cross-flow propellers are characterized by the rotation of several blades around a vertical axis, associated with the rotation of each blade around its own axis. The main advantage of these systems is to generate a 360° vector thrust force that significantly improves the ships maneuverability. One of the most common cross-flow propellers is the Voith-Schneider Propeller (VSP) which is used for many low-speed ships (tug, ferry, buoyage...)[6]. But this system is kinematically limited from its mechanical rotating technology.
In the past, for a marine energies improvement context, a vertical-axis experimental device has been developed at the Research Institute of the French Naval Academy (IRENav). This mechanism is now operating for propulsion purpose at the wave and current tank of Ifremer in Boulogne-sur-Mer. Its innovative specificity is the use of servo-motors enslaved by the main motor to electrically control the

blades rotation. All types of pitch law could therefore be played, blade control is no more limited by a mechanical system. The idea is to generate uncomplicated pitch law defined by a kinematic approach for a target optimization (thrust maximization, efficiency maximization,...). And then correct them taking into account flow effects (curvature of the flow, induced velocity, 3D effects) by using the experimental thruster. This correction provided by experiments is done by a meta-model optimization [7]. This optimization could also be managed by a Computational Fluid Dynamics code (URANS 3D, DNS,...).
The goal of this paper is the presentation and the development of the experimental thruster. The first section of this paper describes the kinematics of the cycloidal propulsion and the pitch definition according quasi-static hypothesis (zero-order laws).
The second section presents Ifremer experimental facilities and the propeller from both mechanical and electrical point of view. Then, first experiments reveal an imprecise pitch law tracking. To deal with this concern, Matlab Simulink simulations have been purchased to calibrate command parameters of speed controllers. Meanwhile, an electronic test bench is developed at the IRENav to investigate new command strategies.

2 Kinematic analysis and pitch law optimization

2.1 Kinematic overview

In this subsection, the kinematic motion of this type of propellers is first describing. For a clear representation and considering that blade length is longer than blade chord, a 2D hypothesis is assumed. In this case, the incoming flow is the combination of the ship speed inverse ($-\overrightarrow{Va}$) and the propeller ortho-radial speed ($\overrightarrow{Vr} = \Omega R\overrightarrow{z}$), Ω is the propeller rotational speed and R the propeller radius. The advance parameter λ is thus defined by :

$$\lambda = \frac{Va}{Vr} \tag{1}$$

Depending on the value of this parameter lambda, two kinematic motions are observed: epicycloid mode ($\lambda < 1$) and trochoidal mode ($\lambda > 1$).

Epicycloidal mode corresponds in case of flow velocity is below the blade ortho-radial velocity. This is the Voith-Schneider operating mode. A representation of the blade path is drawn on the figure 1 (2D representation). The ship is moving towards the left (in $\overrightarrow{Va}$ direction). This mode allows heavy maneuverability and a quick start of the propulsion. However, it is limited to a 15 knots ship speed.

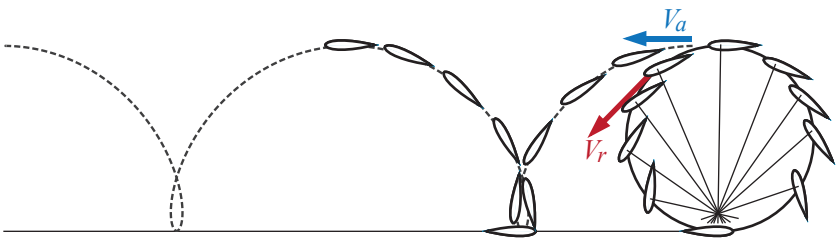

Figure 1 – 2D blade path for the epicycloid mode ($\lambda < 1$)

Trochoid mode corresponds in case of flow velocity is higher than blade ortho-radial velocity. Lipp thruster is operating in this mode. The blade path representation is given on the figure 2 (2D represen-

tation). This mode allows high ship speed (the ship speed is no more limited by the engine rotational speed). Another interesting feature of this mode is the effect of cavitation delaying. But with this type of propulsion, engine starting is more difficult (especially for heavy vessels).

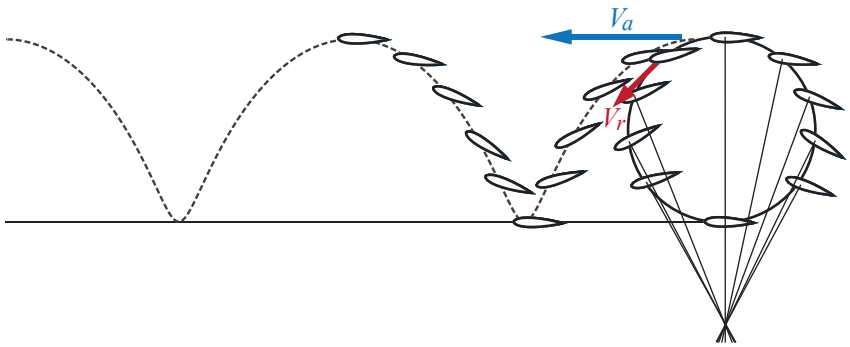

Figure 2 – 2D blade path for the trochoid mode ($\lambda > 1$)

For existing cross-flow technologies, the blade pitch is forced by a mechanical system (connecting rods, gears, crank, camshaft...) connected to the main rotation (principal engine). Thrust magnitude and direction is allowed by geometrical parameters that modify the layout of these mechanical components, translation, and rotation usually. Concerning the experimental thruster presented in this article, the blade pitch is no longer mechanically depending on the main motor rotation. Indeed three servo-motors enslaved by the principal are imposing independent blade pitching (figure 7 shows the 3-blades experimental propeller). This choice of technology guarantees simultaneously the thrust modification in magnitude and direction and also the two λ modes switching by the pitch law adjustment.
Before tackle the propeller description, the next subsection is focusing on the local hydrodynamic forces acting on the blade and the procedure to define the pitch law maximizing for a target optimization (thrust maximization for instance).

2.2 Zero-order pitch law analysis

For this section, the relative velocity viewed by one blade $\overrightarrow{W}$ is considering to be the simple combination of the ship advance $\overrightarrow{Va}$ and the propeller rotational speed $\overrightarrow{Vr}$:

$$\overrightarrow{W} = -(\overrightarrow{Vr} + \overrightarrow{Va}) \tag{2}$$

Figure 3 represents relative velocity magnitude and direction for the cases $\lambda < 1$ and $\lambda > 1$.

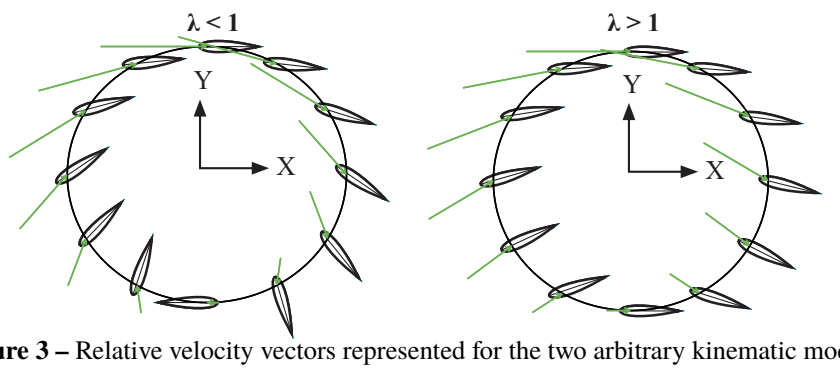

Figure 3 – Relative velocity vectors represented for the two arbitrary kinematic modes

This definition implies strong suppositions on the flow description. The blade pitching velocity is neglected, the relative velocity is calculated at the blade rotation center.

Induced velocities and effects of curvature flow, respectively attributed to the flow acceleration behind the propeller and the rotational speed, are also ignored as the effect of the wake.
These flow modifications have a local impact, especially on the relative velocity direction. Induced and wake velocities might have been estimated by a Blade Element Momentum method (or Double Multiple Stream Tube) [3, 4], but it's not the present work's objective. The relation (2) gives a correct and quick estimation of the relative velocity. This reasoning is called 'zero-order' analysis. According to these assumptions, relative velocity magnitude W and direction i (oriented angle between x-axis and W) are given by equations (3):

$$W = Va.\sqrt{1 + \frac{2cos(\theta)}{\lambda} + \left(\frac{1}{\lambda}\right)^2} \quad ; \quad i = atan\left(\frac{sin(\theta)}{\lambda + cos(\theta)}\right) \tag{3}$$

θ is the orbital position of a blade, $\theta \in [0° : 360°]$, and the rotational speed is given by:

$$\Omega = \dot{\theta} = \frac{d\theta}{dt} \tag{4}$$

Considering these kinematic definitions, relative velocity magnitude and direction are given for each blade orbital positions θ. Thus, a kinematic pitch law can be modeling using SANDIA database which provides drag and lift coefficients for a given NACA foil [8]. These coefficients are experimentally determinate as a function of the Reynolds number and the incidence angle.
Pitch φ, pitch β and incidence angle α are respectively defined as the oriented angle between the x-axis, the ortho-radial speed direction $\overrightarrow{Vr}$, or the flow direction W on the one hand and the blade chord on the other hand.
Figure 4 gives a representation of these angles for an arbitrary position θ, and equations (5) give relations between these angles.
Finally thrust F_X and transverse force F_Y are the projections of lift F_L and drag F_D (given by the SANDIA coefficients) on the x-axis (ship advance direction) and y-axis(transverse direction) (6). These projections are represented in figure 4.

$$\varphi = i - \alpha \quad ; \quad \beta = \varphi - \theta \tag{5}$$

$$F_X = [F_D\ cos(i) - F_L\ sin(i)] \quad ; \quad F_Y = [F_L\ cos(i) + F_D\ sin(i)] \tag{6}$$

$$Re_c = \frac{Wc}{\nu} \tag{7}$$

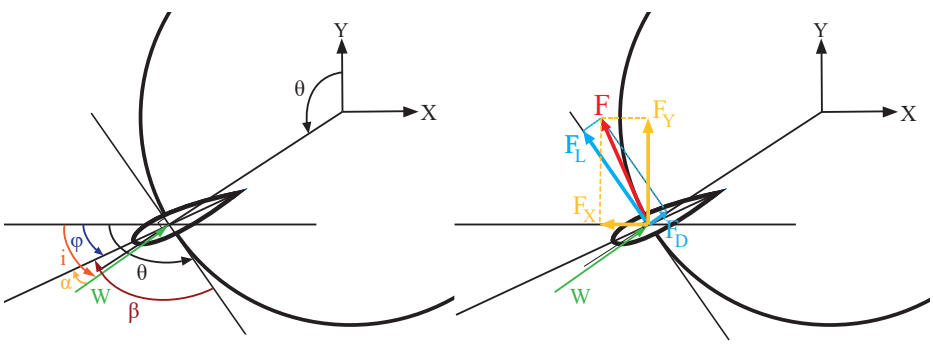

Figure 4 – Angle definitions (left) and hydrodynamic force decomposition (right) for an arbitrary position θ

For each orbital positions θ, knowing relative velocity magnitude W and direction i (3), local Reynolds

number Re_c (7), a large interval of incidence angle α in the SANDIA data base, the optimal incidence can be determined for a target optimization (maximizing F_X, minimizing F_Y,...). By the relation (5), the pitch law is then calculated.
Figure 5 shows zero-order pitch laws for different values of λ in the case of the thrust maximization. The same reasoning could be used for epicycloid mode.

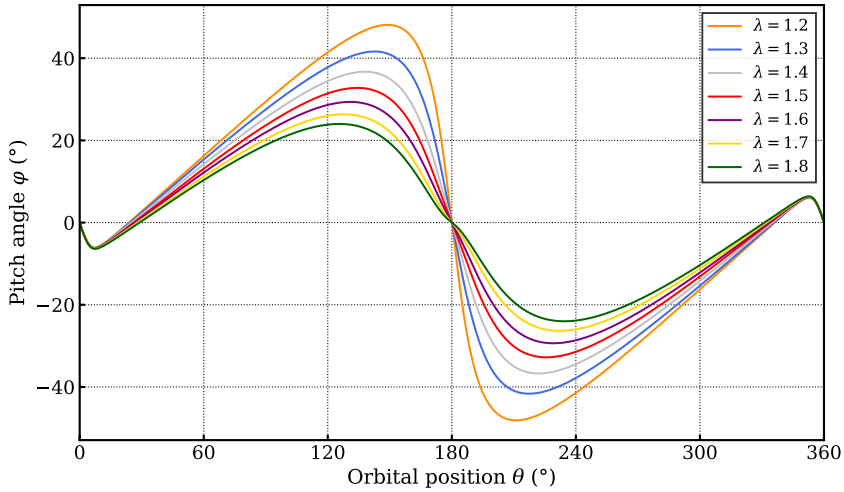

Figure 5 – Optimized pitch laws for different λ values in case of thrust maximization

These pitch laws can then be tested on the thruster at the Ifremer. The next section describes experimental facilities and first measurements collected.

3 Experimental set-up and control optimization

3.1 Ifremer facilities

The Boulogne-sur-Mer Ifremer site owns a wave and current flume tank. The tank working section measures 18 meters long by 4 meters wide and 2 meters depth. An observation window (8 by 2 meters) at one side of the tank allows flow and turbulence model visualization. The figure 6 gives an overview of the Ifremer tank.

Figure 6 – Ifremer wave current flume tank overview

The flow velocity is adjustable from 0.1 to 2.2 m/s with a turbulence intensity controlled between 1.5% and 15%. It is also possible to adjust current profiles.
The flume tank is equipped with measurement systems specific to hydrodynamics. In particular it provides measurements of main mechanical stresses on testing devices and allows to study and visualize the water flow and the dynamical behavior of the models: Laser Dopler Velocimeter (LDV), Particle Image Velocimeter system (PIV), components load-cells (3 or 6), a 3D air and submarine motion tracking system [9].

3.2 Vertical axis blade-controlled thruster

3.2.1 General overview

The experimental thruster is composed of three vertical shafts assembled on a triangular frame rotating by the main motor (figure 7). Each shaft is connected to the frame by a sliding guide which allows the modification of the system diameter. For the propulsion mode, the smallest position ($D = 0.8\ m$) is locked because it leads to the best efficiency according papers. Whereas for marine generator, spaced configuration generates better efficiency. To increase the solidity of the thruster in the smaller configuration, blade chord can be modified by switching blades. Indeed blades are attached to shafts by a clamp tightened with bolts. This system also allows us to switch from a NACA blade profile to an other (asymmetric for instance) or change the blade material to investigate other area of research.
The specificity of this device is its independent blade rotations. Indeed, each blade is controlled by a servo-motor enslaved by the main engine. These secondary engines are located at the top of each blade shaft. A speed reducer (ratio 10) is linked at each engine shaft to limit the torque perceived by the motor and work at the nominal speed.

Diameter ($D = 2R$)	$0.8 - 1.6\ [m]$
Number of blades (N)	3
Entire weight	$650\ [kg]$
Blade span (l)	$1\ [m]$
Blade profile	NACA 0018
Blade chord (c)	$0.15\ [m]$
Blade rotation axis position	1/4 chord
Solidity ($\sigma = Nc/R$)	$0.5625 - 1.125$
Aspect Ratio ($AR = l/c$)	6.7
Chord Radius ratio ($c_r = c/R$)	$0.1875 - 0.375$
Main engine C_{max} ; Ω_{max}	$100\ [Nm]$; $150\ [RPM]$
Secondary engines $C_{i_{max}}$; $\Omega_{i_{max}}$	$40\ [Nm]$; $150\ [RPM]$

Figure 7 – Picture and characteristics of the experimental thruster

3.2.2 Measurement device instrumentation

The experimental propeller leans on two horizontal I-beams which elevate the system above the tank (figure 6); only the blades are under the water line. Four 3D load-cells installed on each beam (two by

beam) measure global hydrodynamic forces which are operating on the device. A torque meter measures the torque on the main shaft. One blade is instrumented with 2D load-cells to measure local forces during the rotation. Table 1 gives measurements ranges and uncertainty of these load-cells (according to the supplier).

Table 1 – Load-cells ranges and uncertainty

	Range	Uncertainty (% of Range)
Fixed 3D load-cells	$F_X \pm 5000\ [N]$	0.8%
	$F_Y \pm 5000\ [N]$	0.22%
	$F_Z \pm 7000\ [N]$	0.54%
Embedded 2D load-cell	$F_{Nb} \pm 5000\ [N]$	0.81%
	$F_{Tb} \pm 1000\ [N]$	1.76%

Load-cells record voltages from their strain gauges and transfer matrices (table 2 for the embedded load-cell) give corresponding forces in Newton.

Table 2 – Transfer matrix for the 2D embedded load-cell

	$P1$	$P1'$	$P2$	$P2'$	$\lvert P1\rvert$	$\lvert P1'\rvert$	$\lvert P2\rvert$	$\lvert P2'\rvert$
F_{Nb}	3298.6	-2813.0	21.9	-20.6	-10.2	6.9	-32.6	34.2
F_{Tb}	-20.9	9.0	-497.8	606.5	-26.3	20.4	-37.6	37.4

For fixed 3D load-cells, forces are directly calculated on the absolute reference frame (X, Y, Z). For the embedded 2D load-cell, forces are given on the blade reference frame (N_b , T_b). Rotation matrix (equation 8) is used to move from (N_b , T_b) to absolute reference frame (X, Y) or rotor reference frame (N, T) moving at the rotational speed Ω=$\dot{\theta}$. Equation (9) gives these relations while figure 8 gives the geometric representation.

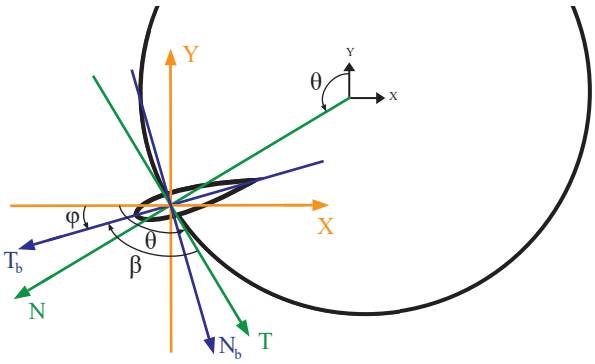

Figure 8 – Reference frames representation for an arbitrary θ position

$$R(\theta) = \begin{pmatrix} \cos(\theta) & -\sin(\theta) \\ \sin(\theta) & \cos(\theta) \end{pmatrix} \tag{8}$$

$$\begin{pmatrix} N \\ T \end{pmatrix} = R\left(\frac{\pi}{2} - \theta\right) \begin{pmatrix} X \\ Y \end{pmatrix} \ ; \ \begin{pmatrix} T_b \\ N_b \end{pmatrix} = R\left(\frac{\pi}{2} + \beta\right) \begin{pmatrix} N \\ T \end{pmatrix} \ ; \ \begin{pmatrix} X \\ Y \end{pmatrix} = R\left(\pi - \varphi\right) \begin{pmatrix} T_b \\ N_b \end{pmatrix} \tag{9}$$

All data are collected by a National Instruments CompactDAQ system plugged to the computer. A Labview code sends the acquisition order (time duration and acquisition frequency) and saves measurements.

3.2.3 Command organization

Figure 9 describes the thruster electrical architecture. It is composed of four permanent magnet synchronus motors (PMSM). The main PMSM (MP) is alimented by a back to back converter, itself powered by a 230/400V network. The speed control of this motor is simply done by two PI controller (one for the speed Ω and one for the intensity).
An other network 120VDC is create through a transformer and a rectifier. This new network powers the three secondary PMSM (MS1, MS2, MS3) which rotating the blades through an inverter. They are controlled in position β_i, depending to the position θ of MP (β_i are tabulated in function of the orbital position θ , each law is $2\pi/3$-dephasing). For these motors, PI controllers are used for intensity and $\dot{\beta}_i$ speed whereas P controller is used for β_i position.

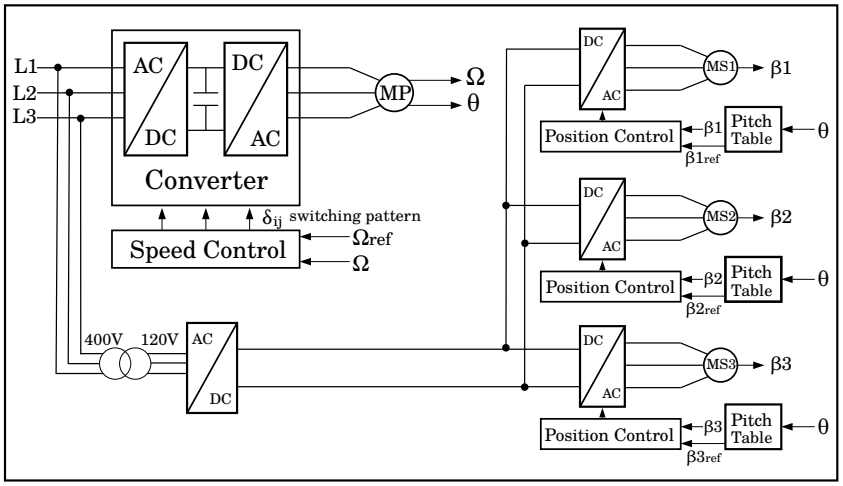

Figure 9 – Electrical diagram of the experimental thruster

MP speed control and MSi position control are supervised by a Labview code through an control human-computer interaction (HCI). This HCI communicates through a controller area network (CAN bus) with the MP converter (TUBA series from Elmo brand) which is installed alongside the Ifremer tank. MSi converters (CELLO series from Elmo brand) are chained on the experimental thruster and interact with the TUBA trough the CAN bus.
The control-HCI retrieves the θ position from the TUBA and sends β_i pitch orders to the three CELLO to achieve position control. TUBA and CELLO get back their positions to the HCI to evaluate the error from the set-point. All these information circulates through the CAN bus with a sampling time of 25 ms.

3.3 Blade-control strategy modification

3.3.1 Experiments observations

After first experiments at Ifremer this year, measurements reveal an unreliable tracking of the main motor speed set-point. Indeed, figure 10 shows differences between reference and the orbital position (left subplot) or the speed velocity (right subplot) during many acquisition laps in the case of the thrust maximization (λ=1.6). Even if the θ position tracking seems correct, the zoom shows an offset between the measurements and the reference. This is due to the main motor rotational speed response which oscillates between 6 RPM and 9 RPM (the set-point is 7.46 RPM).

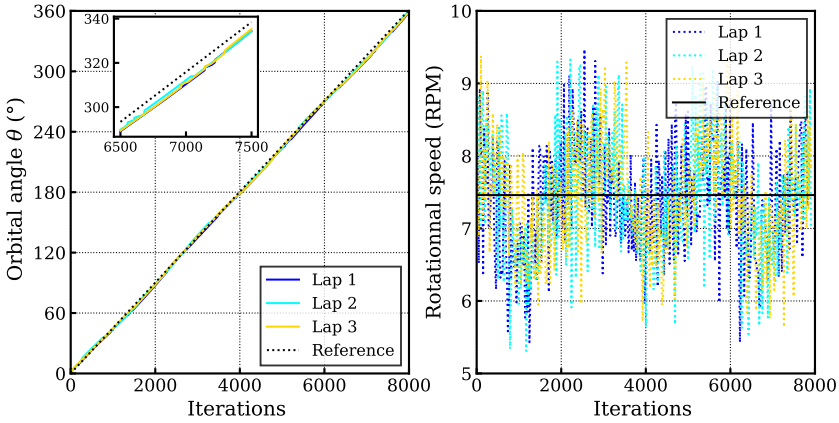

Figure 10 – Measured orbital position θ and rotational speed during three laps

Figure 11 also shows an offset between the reference and experiments on the blade pitch tracking. In addition, oscillations on the blade control are unfavorable for the flow establishment and generate noise on the structure.

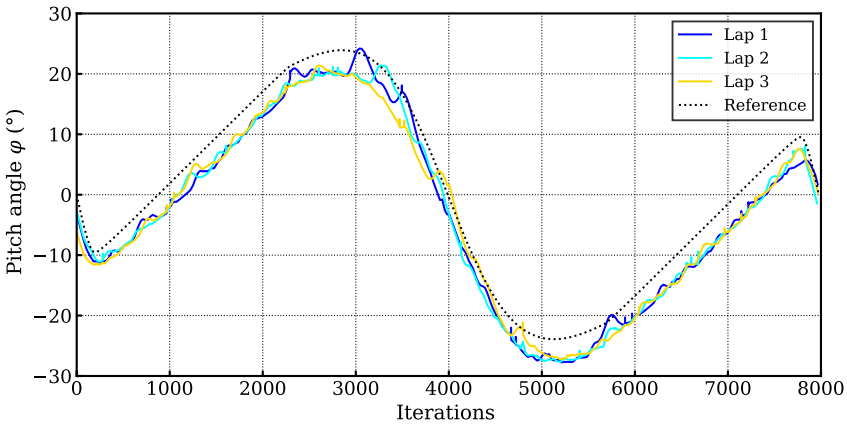

Figure 11 – Pitch law φ measured during three laps

The first explanation of the Ω variation is due to a sliding between the main motor shaft and the triangular frame. This sliding operates when the torque is too high (mostly at the beginning of the rotation or for high rotational speeds). This issue was rectified by inserting pins on the main shaft to mechanically eliminate this sliding. Another issue comes from the PI parameters from converters which has been automatically calculated by the integrated software from Elmo brand when sliding was still appearing. PI parameters have then to be re-calibrated in the next experiments campaign.

In addition, MSi position control is done by only proportional corrector, this leads to an offset of the response in regards to the set-point. This offset can be adjusted by the use of proportional and integrated corrector.

Lastly CAN bus is certainly disturbing information from control procedure. Indeed, the connection between TUBA converter (alongside the tank) and embedded CELLO converters is realized through a slip ring. Electromagnetic interferences can occur in this connection and distort the signal. Finally, MSi controllers feedback loop is limited by the CAN bus acquisition time which is too long (25ms). Indeed, with a rotational speed Ω of 7.46 RPM, orbital angle $\Delta\theta$ covered in a 25ms laps time Δt is over one

degree. That implies a response for secondary engines position controllers above the degree, the control of MSi is then inaccurate, the reference pitch law can't be tracked accurately. Acquisition time of the CAN bus could be decreased less than 10ms but it's not enough. In addition rotational speed is low for this experiment test (the flow speed is 0.5m/s and λ>1),whereas for epicycloid mode (λ<1) rotational speed is faster (about 30 RPM for λ=1.6 and flow velocity of 1m/s).

3.3.2 Modifications

Speed controllers parameters were adjusted by electrical simulations on Matlab Simulink, for the position control of MSi, an integrated corrector has been added. Figure 12 gives results from this simulation (red triangles) in comparison with the controllers parameters given by first measurements (yellow line). With readjusted PI parameters the response perfectly fit the reference law, the offset of blade pitch tracking (zoom at the right figure 12) is fixed. The same improvement is done on the MP speed control.

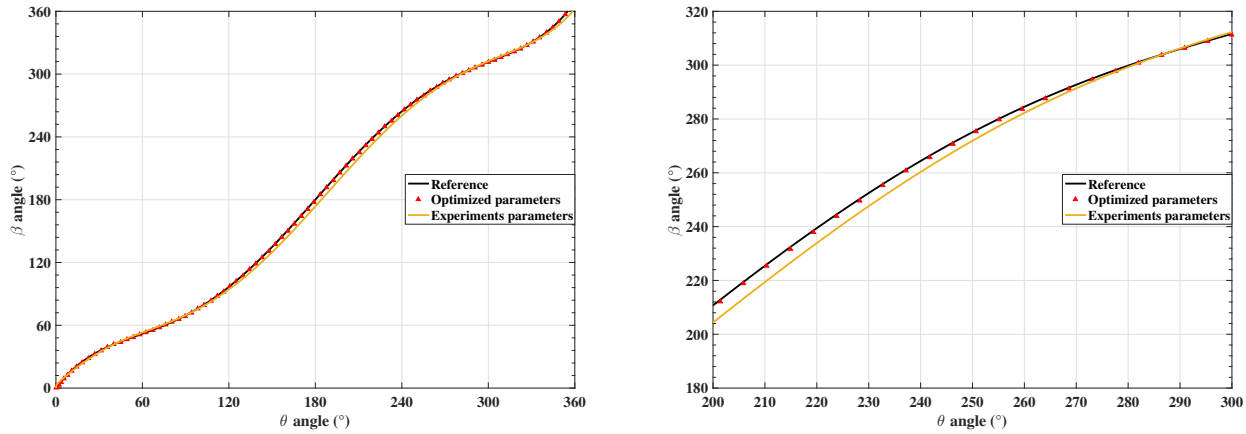

Figure 12 – Blade-control comparison on β between experiments controller parameters and Matlab Simulink parameters. At the right, zoom on the x-axis.

Moreover, the CAN bus control has been replaced by an embedded control drive by a micro-controller unit(MCU) plugged on the thruster. This MCU, in which pitch laws reference are stored, send directly command orders to the MSi controllers. The orbital position θ is given by a rotary encoder fixed on the triangular frame and connected to the MCU. Embedded CELLO converters communicate with the MCU with an analogical language faster than CAN bus (sampling time about 10^{-6}s). This improvement also avoids control information transit between the computer and the thruster, the feedback loop of MSi is directly performed inside the embedded MCU.
A test bench (figure 13) is developed at the IRENav nowadays to configure and test this technology improvement before next experiments scheduled in July.

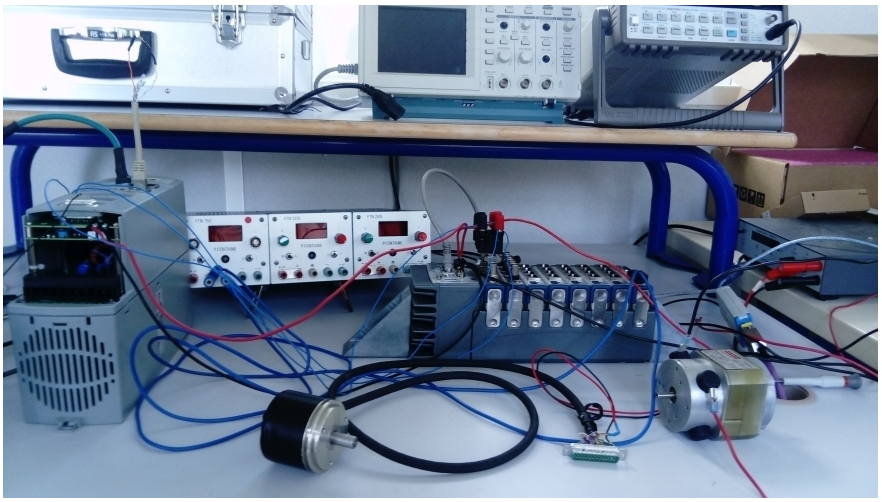

Figure 13 – Test bench developed at the IRENav to configure new blade-control strategy

4 Conclusion & Perspectives

This article has presented the development of the experimental blade-controlled cycloidal propeller designed at the French Naval Academy Institute and Ifremer. First experiments campaign reveals the need of speed control improvement. Indeed the blade-control tracking is inaccurate for our experiments expectations. Electronic simulations are then initiated to numerically drive the thruster and correct controllers parameters.

Meanwhile, a new command strategy has been taken with the use of an embedded micro controller to handle directly blade pitch rotation. A test bench is developed at the IRENav to configure and adapt this technology on the existing platform.

Next experiments will confirm this new command strategy with a reliable pitch motion tracking expectation. These experiments will also test zero-order laws developed in this article and allow the investigation of the optimization procedure.

5 Acknowledgments

We would like to thank all members of the Boulogne-sur-Mer Ifremer Institute for hosting our team in their laboratory and for their valuable support.

We also thank the SCEFER (Service Conception Etude et Fabrication pour l'Enseignement et la Recherche) for the support in technical issues since the beginning of the project with a special gratitude to Alain Boulch, electrotech-engineer at the IRENav, for developing all the Labview code.

A last acknowledgement is addressed to the student Emmanuel Delaire who has simulated the electrical version of the thruster on Matlab Simulink.

References

[1] Frédéric Hauville, Romain Lecuyer-Le Bris, François Deniset, and Guillaume Fasse. Pitch law optimization of a cycloidal propulsor. In *16e Journées de l'Hydrodynamique, Marseille, France*.

[2] Benoît Paillard, Frédéric Hauville, and Jacques Andre Astolfi. Simulating variable pitch crossflow water turbines: A coupled unsteady onera-edlin model and streamtube model. *Renewable Energy*, 52:209–217, 2013.

[3] Benoit Paillard. *Simulation numérique et optimisation d'une hydrolienne à axe transverse avec contrôle actif de l'angle de calage*. PhD thesis, Brest, 2011.

[4] Pierre-Luc Delafin. *Analyse de l'écoulement transitionnel sur un hydrofoil: application aux hydroliennes à axe transverse avec contrôle actif de l'angle de calage*. PhD thesis, Brest, 2014.

[5] DS Barrett, MS Triantafyllou, DKP Yue, MA Grosenbaugh, and MJ Wolfgang. Drag reduction in fish-like locomotion. *Journal of Fluid Mechanics*, 392:183–212, 1999.

[6] Jens-Erk Bartels and Dirk Jürgens. The voith schneider propeller: Current applications and new developments. *Heidenheim: Voith Publication*, 2006.

[7] Matthieu Sacher, Frédéric Hauville, Régis Duvigneau, Olivier Le Maître, Nicolas Aubin, and Mathieu Durand. Efficient optimization procedure in non-linear fluid-structure interaction problem: Application to mainsail trimming in upwind conditions. *Journal of Fluids and Structures*, 69:209–231, 2017.

[8] Robert E Sheldahl and Paul C Klimas. Aerodynamic characteristics of seven symmetrical airfoil sections through 180-degree angle of attack for use in aerodynamic analysis of vertical axis wind turbines. Technical report, Sandia National Labs., Albuquerque, NM (USA), 1981.

[9] Bachar Mallat, Grégory Germain, Benoit Gaurier, Philippe Druault, and Jean-Yves Billard. Experimental study of the bubble sweep-down phenomenon on three bow designs. *Ocean Engineering*, 148:361–375, 2018.